

Supplementary Materials

Enhanced Photo-Assisted Lithium-Ion Batteries Using Natural Dye- Impregnated LiFePO₄ Cathodes

Can Cui ^a, Beili Pang ^{a, *}, Song Xu ^a, Jianguang Feng ^a, Hongzhou Dong ^a, Mingwei Shang ^{b, *},

Liyan Yu ^{a, *}, Lifeng Dong ^{a, c, *}

^a College of Materials Science and Engineering, Qingdao University of Science and
Technology, Qingdao 266042, China

^b Wuxi Zero to One to Future New Material Research Institute Co., Ltd., Wuxi, Jiangsu

^c Department of Physics, Hamline University, St. Paul 55104, USA

E-mail: pangbl@qust.edu.cn; shangmingwei@yanyii.cn; liyanyu@qust.edu.cn;
donglifeng@qust.edu.cn

1. Supporting Methods

1.1 Material Preparation

LFP, super carbon, polyvinylidene fluoride (PVDF, $-(\text{CH}_2-\text{CF}_2)_n-$, 99.5%), and 1 M LiPF_6 electrolyte in ethylene carbonate/dimethyl carbonate (1:1 Vol%) were purchased from Guangdong Canrd New Energy Technology Ltd. Turmeric powder, N719 powder, and 1-methyl-2-pyrrolidone (NMP, $\text{C}_5\text{H}_9\text{NO}$, 99.0%) were supplied by Shanghai Macklin Ltd.

1.2 Cathode Preparation

The cathode of the LIBs was prepared by mixing 0.8 g LFP, 0.1 g super carbon, and 0.1g PVDF in 2 g NMP to form a slurry. The slurry was uniformly coated onto aluminum foil or mesh collectors via a scraping method, followed by drying at 60 °C. Photoelectrodes were obtained by immersing the LFP cathode in an ethanol solution containing dye molecules for 24 h.

1.3 Design and Assembly of Photo-Assisted LIBs

To simulate sunlight illumination, a 5 mm diameter aperture was created in the positive casing of the CR2032 button battery, sealed with epoxy resin and glass. The dye-impregnated cathode was positioned inside the illuminated positive electrode casing, followed by the addition of the electrolyte, separator, and lithium metal anode. The button batteries were assembled under an argon atmosphere in a glove box using standard procedures.

1.4 Characterizations

Fourier transform infrared (FTIR) spectroscopy was performed using a Nicolet IS10 instrument to identify functional groups in the samples. X-ray diffraction (XRD) analysis was conducted using a Rigaku Smart Lab SE Automated Multipurpose XRD instrument equipped with $\text{Cu K}\alpha$ radiation to examine the crystal structure of the samples. Scanning electron microscopy (SEM) was performed using a Regulus 8100 instrument to characterize the sample morphology. Transmission electron microscopy (TEM) images were acquired with a JEM-2100 PLUS microscope. Surface elemental composition was analyzed via synchronous illumination X-ray photoelectron spectroscopy (SI-XPS) using a Thermo Fisher ESCALAB 250XI instrument. The absorption spectrum of the dye was tested using an ultraviolet-visible spectrophotometer (UV-3900, Hitachi).

Simulated sunlight illumination was provided using a AAA solar simulator (model 7IS0503A, Beijing Saifan Optoelectronic Instrument Co., Ltd.) with an intensity of 1 sun (100 mW cm^{-2}). Electrochemical measurements, including cyclic voltammetry (CV) and electrochemical impedance spectroscopy (EIS), were conducted on a Metrohm Autolab electrochemical workstation. Constant current charge/discharge testing was carried out using a LAND battery testing system (Wuhan Land Electronics).

1.5 Theoretical Simulations

Density functional theory (DFT) calculations were performed using the Gaussian 09 program. The geometric structure of turmeric molecules was optimized using the restricted B3LYP hybrid functional and 6-31G (d, p) basis set.¹ Molecular orbital analysis focused on the highest occupied molecular orbital (HOMO) and lowest unoccupied molecular orbital (LUMO) energies to evaluate electronic properties.

2. Supporting Tables and Figures

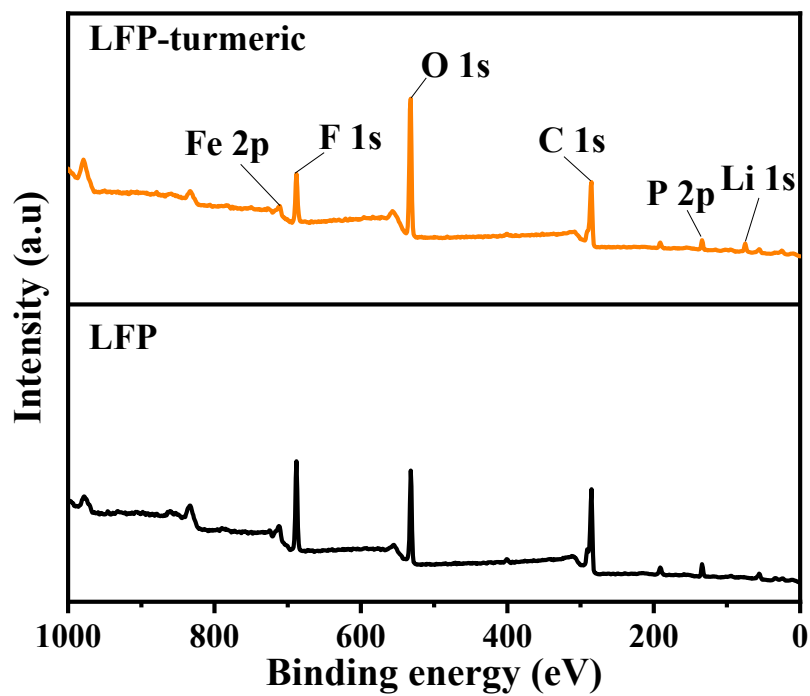


Fig. S1. XPS survey spectra of the electrodes before and after turmeric impregnation.

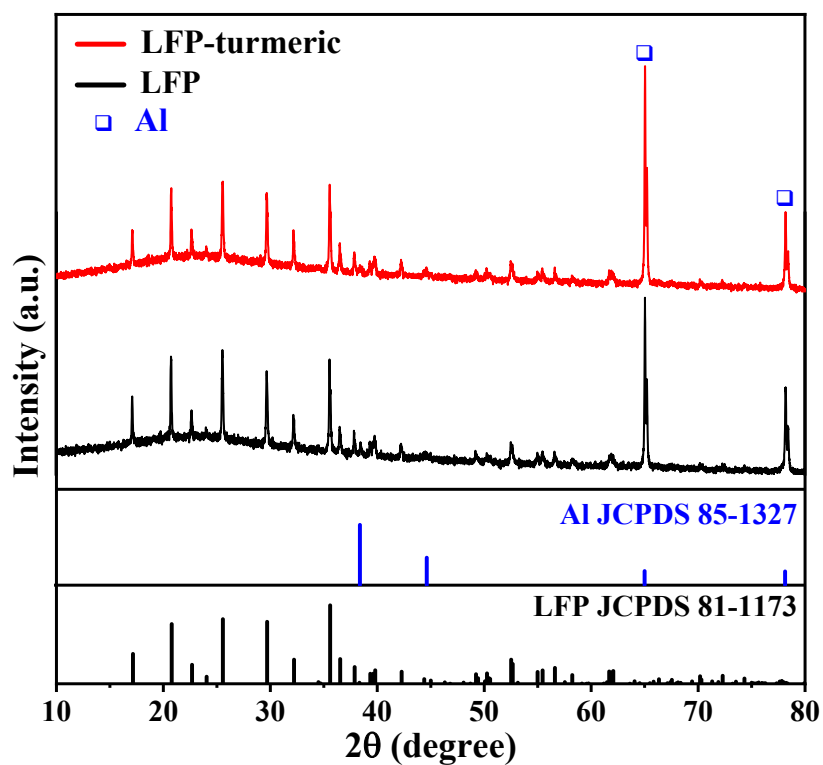


Fig. S2. XRD patterns of the electrodes before and after turmeric impregnation, indicating preserved crystal structure following dye incorporation.

Table S1. Charging and discharging capacities of batteries with different electrodes.

Electrodes	LFP	LFP-turmeric
0.2 C	150.5/150	175.4/171.4
0.5 C	138.5/136.5	165.6/165.6
1 C	122/120.5	154.5/153.6
2 C	100/99	135.7/135.3
5 C	73/74	104/104

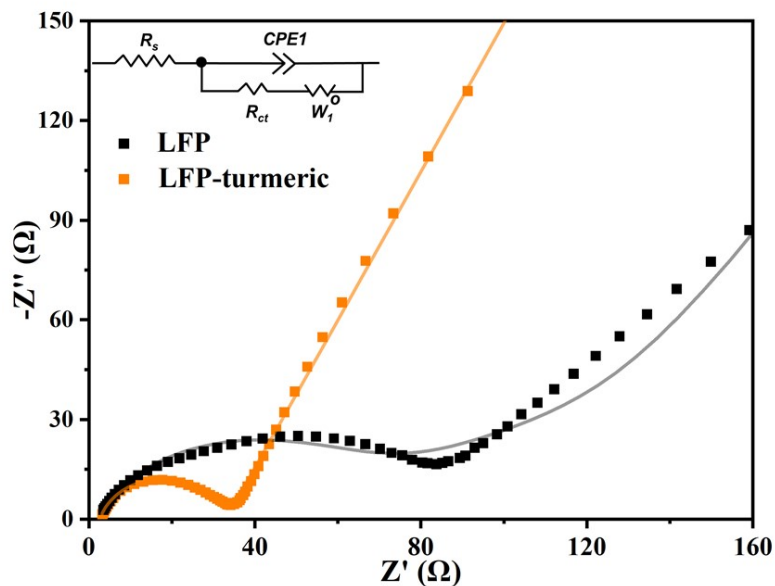


Fig. S3. EIS spectra of the electrodes, along with the equivalent circuit model used for fitting the data.

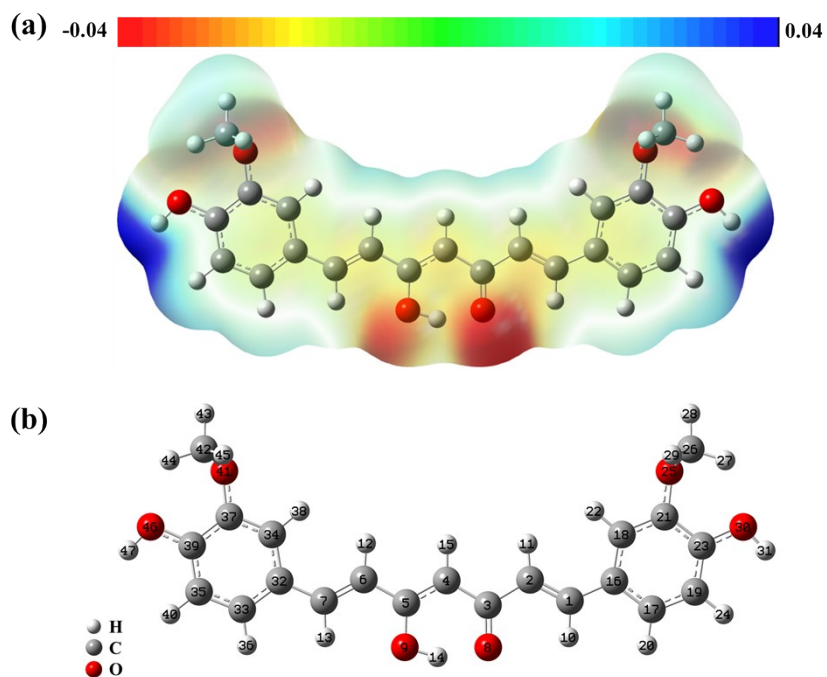


Fig. S4. (a) Molecular electrostatic potential (MESP) map of the turmeric molecule, illustrating regions of electron density; (b) Mulliken charge population distribution, highlighting charge localization on functional groups

Table S2. Calculated Mulliken atomic charges for all atoms in the turmeric molecular system.

Atom No.	Atom Type	Mulliken Charge
1	C	-0.10387
2	C	-0.13566
3	C	0.422707
4	C	-0.23511
5	C	0.388765
6	C	-0.12747
7	C	-0.11182
8	O	-0.60661
9	O	-0.5621
10	H	0.11718
11	H	0.079888
12	H	0.087868
13	H	0.117467
14	H	0.371644
15	H	0.079605
16	C	0.127351
17	C	-0.13469
18	C	-0.14696
19	C	-0.13721
20	H	0.094847
21	C	0.314052
22	H	0.09556
23	C	0.306582
24	H	0.082085
25	O	-0.52932
26	C	-0.08201
27	H	0.125829
28	H	0.119256
29	H	0.10128
30	O	-0.55036
31	H	0.322455
32	C	0.129065
33	C	-0.13585
34	C	-0.148
35	C	-0.13675
36	H	0.093747
37	C	0.314143
38	H	0.095411
39	C	0.306252
40	H	0.082475
41	O	-0.52911
42	C	-0.08234
43	H	0.119679
44	H	0.126229
45	H	0.101459
46	O	-0.55026
47	H	0.322611

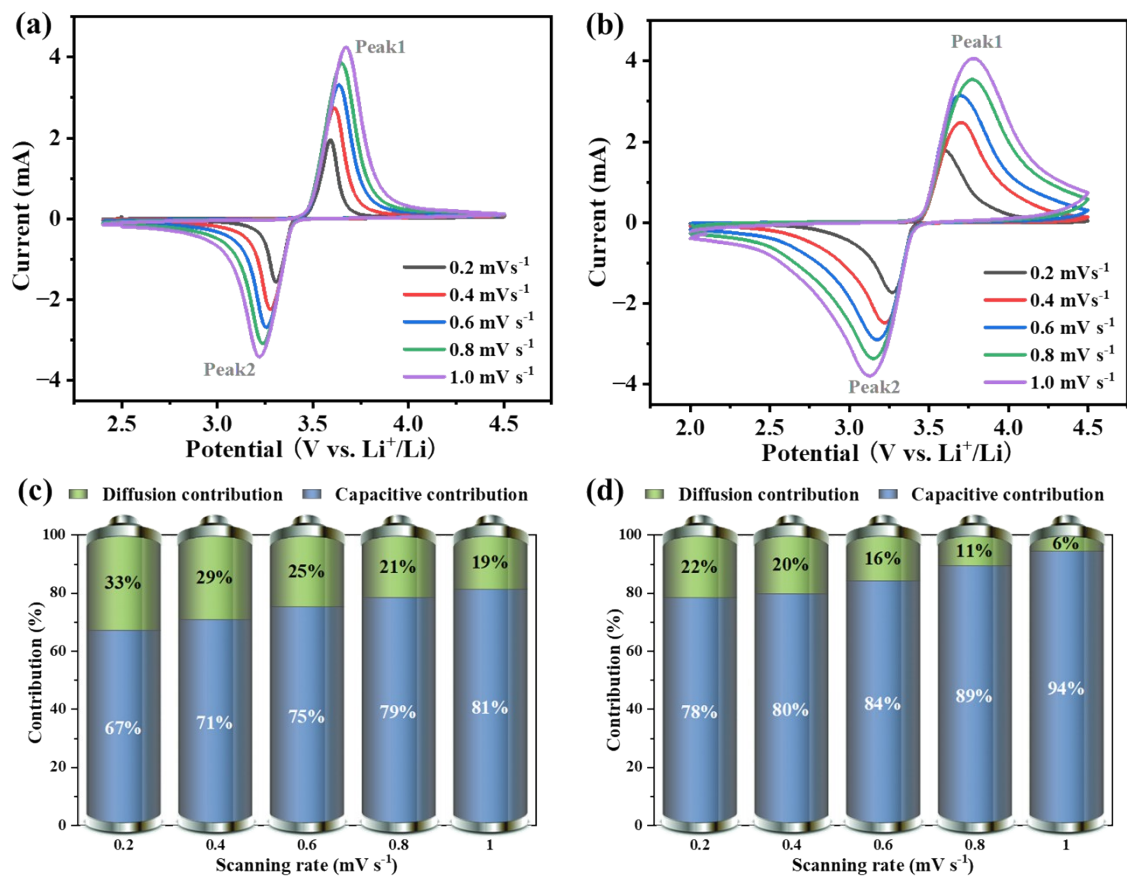


Fig. S5. CV curves recorded at scan rates from 0.2 to 1.0 mV s⁻¹ for (a) pristine LFP and (b) LFP-turmeric electrodes. Capacitive and diffusion-controlled contributions for (c) LFP and (d) LFP-turmeric.

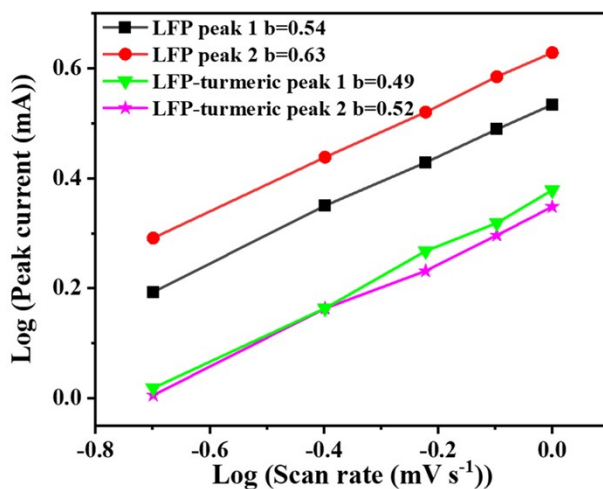


Fig. S6. Determination of b values for cathodic and anodic peaks.

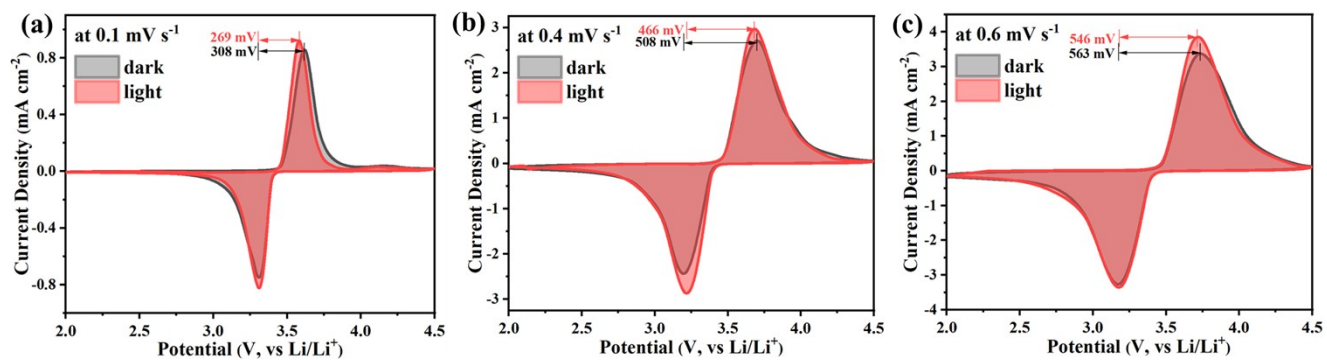


Fig. S7. CV curves of the LFP-turmeric electrode at 0.1, 0.4 and 0.6 mV s⁻¹ under dark and illuminated conditions.

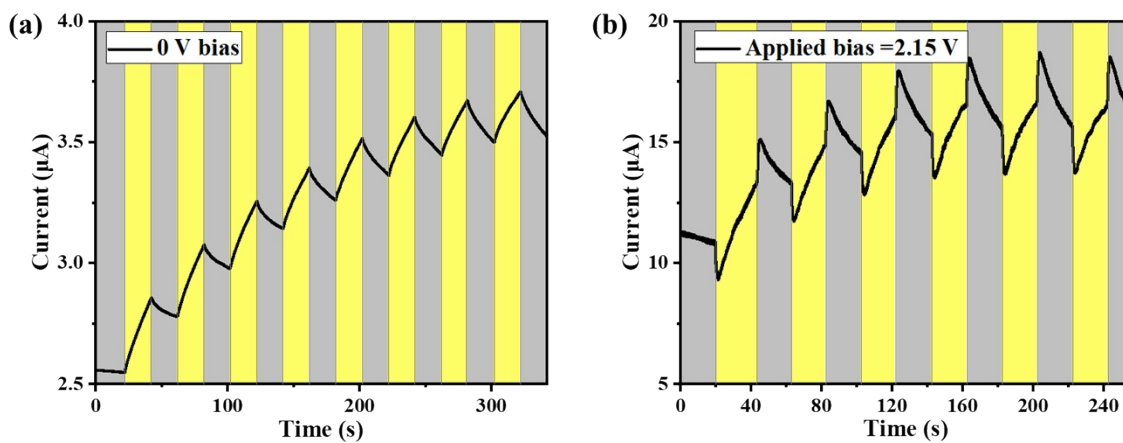


Fig. S8. Photocurrent response of the LFP-turmeric electrode (a) without external bias and (b) under applied bias voltages. Yellow stripes indicate periods of illumination; grey stripes represent dark conditions.

Table S3. Resistance fitting parameters for different composites obtained from EIS analysis.

Samples/Condition	R_s (Ω)	R_{ct} (Ω)
LFP	2.02	60.36
LFP-turmeric-dark	2.80	30.89
LFP-turmeric-light	2.86	28.47

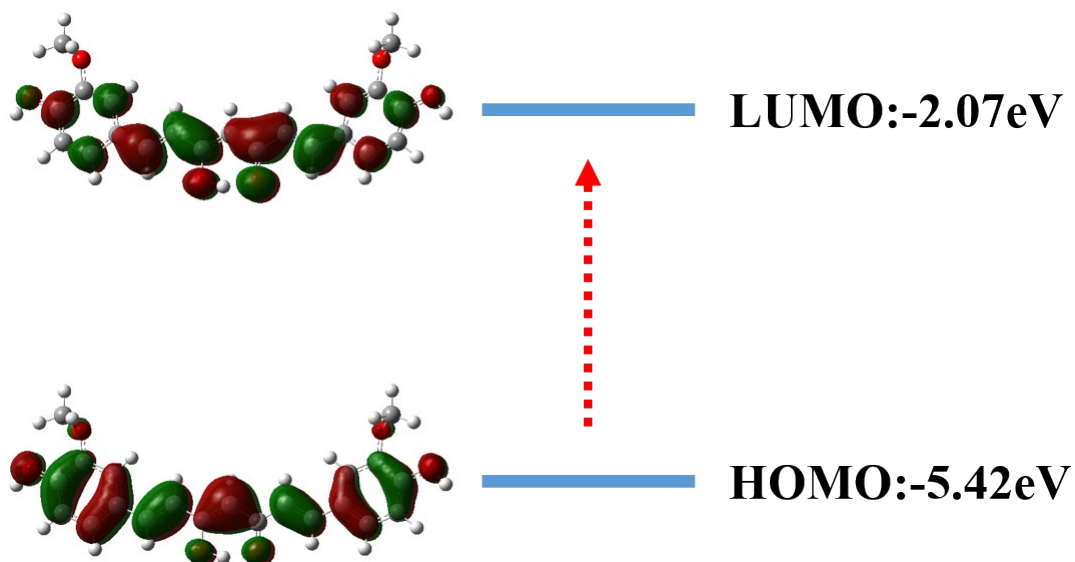


Fig. S9. Simulated HOMO and LUMO distributions of turmeric.

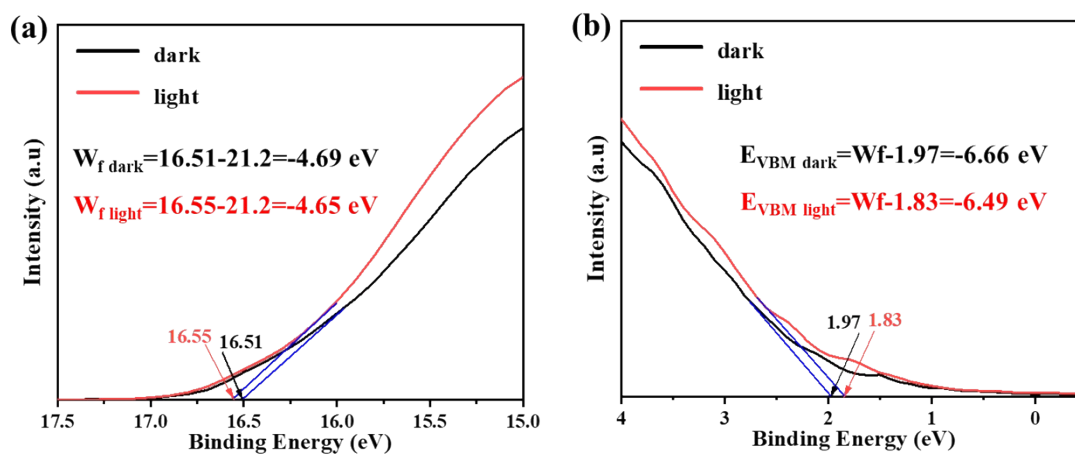


Fig. S10. (a) Photoemission cutoff spectra of turmeric; (b) Valence band structure of turmeric.

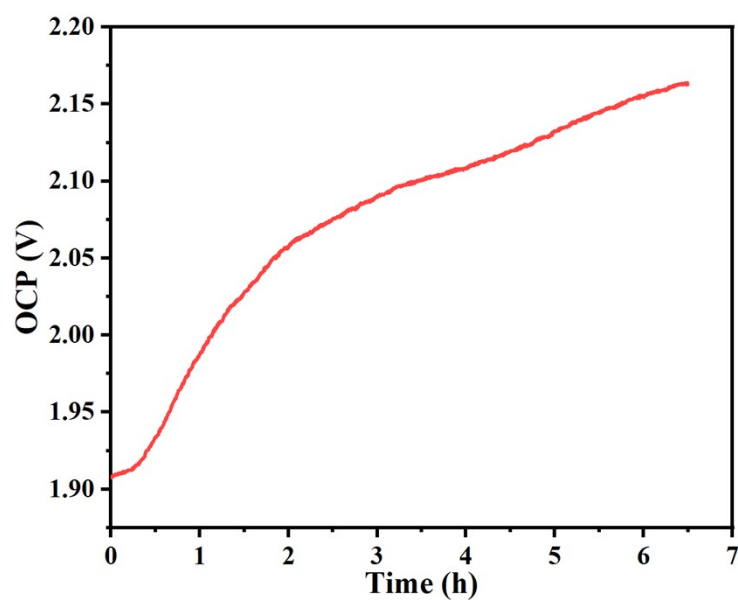


Fig. S11. Open circuit potential of the LFP-turmeric photo-assisted battery under light irradiation.

Reference

1. J. Lee and M. J. Park, *Adv. Energy Mater.*, 2017, 7, 1602279.